International Journal Of
Industrial Electronics Control and Optimization
Print ISSN: 3517-2645
Online ISSN: 3568-2645
Homepage: https://ieco.usb.ac.ir/

Novel Sliding Mode Control Approach for Quasi-Z-Source Converters with Improved Performance

Gholamreza Shahabadi[1] | Majidreza Naseh[2]

Department of Electrical Engineering, University of Applied Science and Technology, South Khorasan Branch, Iran[1]
Department of Electrical engineering, Birjand Branch, Islamic Azad University, Birjand, Iran[2]
Corresponding author's email: naseh@iaubir.ac.ir

Article Info

Article type:
Research Article

Article history:
Received: 27-January-2024
Received in revised form: 15-May-2024
Accepted: 21-May-2024
Published online: 22-Sep-2024

Keywords:
Z-Source,
Quasi-Z-Source,
Sliding mode Control,
Robust control.

ABSTRACT

Quasi-Z-source converters (QZSC) are gaining popularity because they operate in a single stage, use smaller components, and maintain continuous input current with a common ground. This converter is widely used in various applications that require a DC-DC converter. The small-signal analysis and linearization methods are often employed for controlling the Quasi-Z-source converters. The linear model of QZSC does not provide sufficient stability control over a wide range. Sliding Mode Control (SMC) is widely used in electronic power converters due to its variable structure. This paper presents a SMC for a QZSC with three objectives:1) to achieve stability across a wide range of QZSC; 2) to systematically select the proposed controller coefficients; and 3) to enable tracking of the reference voltage in spite of changes in input voltage, reference voltage, and output load. The simulations have been done with the help of MATLAB/Simulink and show the effectiveness of the proposed method.

I. Introduction

As the demand for energy grows, humanity is seeking for new ways to produce electricity on a large scale to satisfy the demands of industrial projects. Due to the limitations and risks associated with electricity generation with fossil resources and nuclear fuel, these approaches are not suitable solutions for supplying electrical power. One of the most effective methods for generating electricity is the use of renewable sources, like solar and wind energy [1, 2]. A DC-DC converter is essential because of the low voltage level and DC output from these sources [3]. Today, the use of DC-DC converters in medical equipment, power factor correction (PFC), electric vehicles, uninterruptible power supply (UPS), green energy systems, portable electrical equipment, photovoltaic systems, wind turbines, fuel cell systems, x-ray systems, auxiliary power supplies, and discharge lamps is commonplace [4, 5].
The Z-source converter (ZSC) is one of the widely used non-isolated converters. It is capable of converting power across AC-DC, AC-AC, DC-AC, and DC-DC configurations [6]. The Quasi-Z-Source converter (QZSC) is a variant of the ZSC and

shares its characteristics. QZSC has all the same characteristics as ZSC. This converter is notable for its broad voltage range, great protection from electromagnetic interference, and immunity to short-circuiting [7]. QZSCs have lower voltage and current stresses, and a higher voltage gain than ZSCs. Recently, various configurations based on the traditional QZSC have emerged [8]. Each configuration is designed for particular applications [9, 10]. Considering the changes in various model parameters in electronic power converters across a wide operating range, the closed-loop control of these converters is a field of research. To effectively design the controller, it is essential to utilize the state-space model of the converter. To derive the system's state-space model, the averaged state space method has been employed. [11]. The adapted state space model is a non-linear model because of the presence of various non-linear components in the structure of converters. Different nonlinear control techniques, such as passivity-based control [12], feedback linearization [13], sliding mode control [14], and adaptive control [15], can be utilized to adjust the output voltage, providing an appropriate response to this issue. Considering the variable structure of power electronic systems and the simplicity of their design, the sliding mode control method can be an appropriate choice for controller design. The initial step in the development of the controller is choosing the sliding surface. The sliding surface can be defined from the combination of system state variables [16]. The goal here is to use a zero-sliding surface to find the control input that will place the system response on the sliding surface. To prevent chattering and limit switching frequency, an adjustable range of bandwidths around the sliding surface is chosen to determine the switching frequency [17].

The most important defect of this method is the change of switching frequency, which has been used to solve this defect by the design method of equivalent control and soft switching [18]. In the equivalent control method, it is necessary to select the derivative of the sliding surface as zero, in addition to the sliding surface itself. Consequently, the controller design assumes that the derivative of the sliding surface is zero. The equivalent control method in controller design involves experimenting with different parameters of the model until the desired output is achieved. In [19], an adaptive sliding model-based equivalent control method is employed to design the controller for the ZSC. During the controller's design, the influence of the output filter within the circuit was not considered. The design process that employs the aforementioned method is highly complex and involves a substantial amount of calculations. In [20], control is conducted by utilizing the definition of hysteresis band based on the feedback linearization control method. In this article, the hysteresis band is not clearly defined, resulting in disruption of the control operation. In [21], the controller for the converter was designed using the sliding step-back control method. By utilizing a trial-and-error approach, the control parameters for this article have been determined. The design procedure in the mentioned method is complex and requires a high number of calculations. In [22], the linearization method is employed to design the controller; however, this does not guarantee stability in a wide range. In [23], the sliding mode controller design method is employed for controller design. In the design of the controller in this method, the effect of the output filter, which is used to eliminate electromagnetic noise, has not been considered. In [24], the sliding mode control technique is employed to design the controller. This study does not examine the impact of variations in the reference voltage on the output. Also, the time required to reach the steady state in tracking the reference voltage is long. In [25], a predictive controller is employed to design the controller. The advantage of these controllers is that they can track sinusoidal currents with near-zero error. This controller has been engineered to function at a specific point within the set, which precludes it from exerting control across a wider range. Based on the presence of a right-sided zero in the voltage transfer function of the capacitor to the duty cycle, it can be inferred that the system is a nonminimum-phase system. Utilizing the duty cycle for directly adjusting the capacitor voltage leads to instability within the closed loop [26]. In order to address this problem, a forward feedback strategy has been suggested in [27]. In this reference, the adjustment of the duty cycle value is based on the steady-state error. The primary limitation of this approach is the substantial error that exists throughout a wide range of converter performance. In [28], a sliding mode controller has been designed. This controller has three drawbacks. Firstly, in order to calculate the reference current of the inverter, it requires access to the load value, which adds the need for incorporating a sensor into the structure. Secondly, the designed controller is of hysteresis type, which leads to variable frequency. Thirdly, the sliding mode controller is designed based on ideal equations, which may not hold valid in persistent state situations. In [29], the design and simulation of a neural sliding mode controller for the electric vehicle's braking system are detailed. This controller exhibits superior performance relative to that of the conventional PI controller. In [30], proposes a solution to overcome the aforementioned three issues. In this reference, an ultra-surface is introduced to regulate the DC voltage and mitigate the nonminimum-phase behavior of the capacitor voltage on the DC side. Additionally, there is no need to separately calculate the reference current of the inductor. This controller, being designed based on a nonlinear model of the converter, offers the capability to operate over a wide range. However, the effects of input voltage variations and load changes on the output voltage of the converter are not addressed in this reference. Additionally, the adjustment of seven parameters is necessary to attain zero steady-state error in the reference output voltage. Consequently, this issue leads to an amplification of computational complexity and a deceleration in the tracking operations. This research presents a novel step-by-step design method for a robust sliding mode controller in a DC-DC QZSC. The parameters of this controller are systematically determined, and then stability analysis is conducted. The design process for controlling the DC-DC flyback converter is discussed in [31]. In [32, 33], new structures of converters are presented with the aim of increasing voltage efficiency. From a control perspective, these converters, with increased voltage gain and a higher number of components, introduce more complexity in the control operation. Apart from the introduction, this article is comprised of the following sections: In the second section, the topology and averaged state-space model of the QZSC are discussed. The third section focuses on the small-signal model of the targeted converter. The fourth section describes the transfer functions of the QZSC using the small-signal model. In the fifth and sixth sections, linear and nonlinear controllers are proposed for the QZSC. The seventh section presents simulations and examines the system's response to variations in reference voltage, load changes, and input voltage variations. Finally, in the eighth section, a summary and conclusion are provided.

II. Topology and state-space model of QZSC

The QZSC has a topology as shown in Figure (1). This circuit consists of capacitors C_1 and C_2, as well as inductors L_1 and L_2. Additionally, this circuit includes a diode and a power switch, denoted as D_1 and S, respectively. In order to reduce noise in the output of this circuit, a capacitor-inductor filter is utilized, with L_f and C_f representing the respective components. The output load is denoted by R_L. In this circuit, V_{in} represents the input voltage, while V_o represents the output voltage of the converter. i_L represents the current flowing through the impedance network inductor, while i_{Lf} denotes the current flowing through the output filter. Moreover, v_{C1} denotes the voltage across the capacitors associated with the QZSC, while v_{Cf} represents the voltage across the capacitor of the output filter. To analyze this converter, it is crucial to consider the following key points:

All components are assumed to be ideal, including the control switch, which is of the MOSFET type.

The converter operates in continuous conduction mode, and its performance is analyzed during steady-state operation.

The capacitance of the capacitors is high enough to disregard the ripple voltage across them.

The state equations of the converter are derived from both the ON and OFF states of the switch. By examining these two states, we can obtain the final state equations of the converter using the method of averaging the state equations.

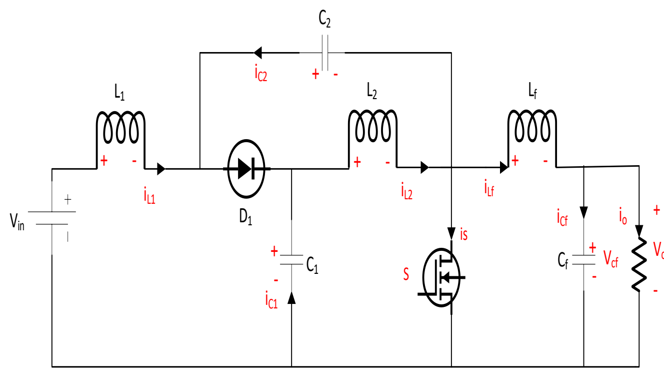

Fig. 1. Configuration of QZSC

III. Analysis of the QZSC in the ON switch state

Figure (2) illustrates the state associated with the switch being in the ON position. In this state, the diode in the converter is OFF. During this state, the capacitors associated with the impedance network in the converter start charging the inductors of the impedance network. In this case, by composing suitable equations, the state equations can be represented as equation (1).

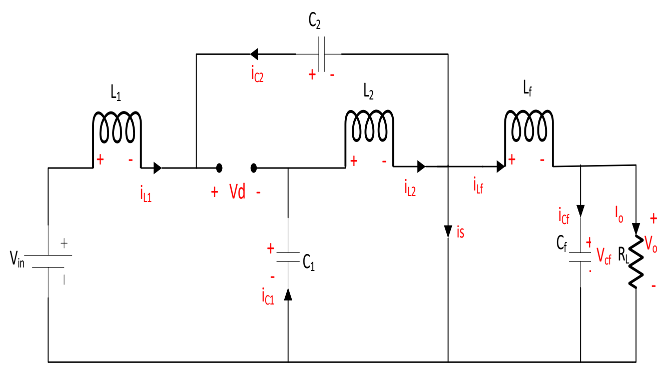

Fig. 2. Configuration of QZSC in ON switch state

$$\begin{cases} L_1 \frac{di_{L1}}{dt} = V_{in} + v_{C2} \\ L_2 \frac{di_{L2}}{dt} = v_{C1} \\ L_f \frac{di_{Lf}}{dt} = -v_{Cf} \\ C_1 \frac{dv_{C1}}{dt} = -i_{L2} \\ C_2 \frac{dv_{C2}}{dt} = -i_{L1} \\ C_f \frac{dv_{Cf}}{dt} = i_{Lf} - \frac{v_{Cf}}{R_L} \end{cases} \quad (1)$$

IV. Analysis of the QZSC in the OFF-switch state

The state depicted in Figure (3) corresponds to the OFF state of the switch. In this state, the energy stored in the inductors of the impedance network is transferred to the capacitors. The diode is in a forward-biased state during this condition. As a result, by formulating suitable equations, the state equations can be expressed as equation (2).

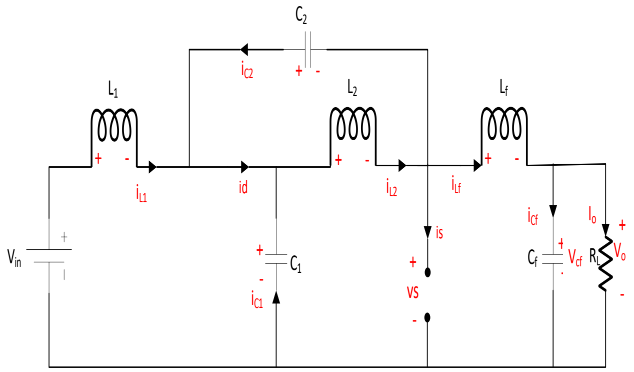

Fig. 3. Configuration of QZSC in OFF switch

$$\begin{cases} L_1\frac{di_{L1}}{dt}=V_{in}-v_{C1} \\ L_2\frac{di_{L2}}{dt}=-v_{C2} \\ L_f\frac{di_{Lf}}{dt}=v_{C1}+v_{C2}-v_{Cf} \\ C_1\frac{dv_{C1}}{dt}=i_{L1}-i_{Lf} \\ C_2\frac{dv_{C2}}{dt}=i_{L2}-i_{Lf} \\ C_f\frac{dv_{Cf}}{dt}=i_{Lf}-\frac{v_{Cf}}{R_L} \end{cases} \quad (2)$$

By applying the principle of the second voltage balance to the inductors, we can obtain the following equations (3):

$$\int_0^{DT_s} i_{L1}dt+\int_{DT_s}^{T_s} i_{L1}dt=0$$
$$\int_0^{DT_s} i_{L2}dt+\int_{DT_s}^{T_s} i_{L2}dt=0$$
$$\int_0^{DT_s} i_{Lf}dt+\int_{DT_s}^{T_s} i_{Lf}dt=0 \quad (3)$$

In equation (3), the coefficient D represents the duty cycle, which is the ratio of the switch-on time or the duration of the short connection period to the total time of one switching cycle. By applying the principle of the second voltage balance to the inductors, the gain of the converter in the steady state can be calculated as equation (4).

$$\frac{v_{Cf}}{V_{in}}=\frac{1-D}{1-2D} \quad (4)$$

V. Averaged state-space model of QZSC

The final state equations of the system are derived by multiplying the state equations corresponding to the switch-on state by the coefficient D, and multiplying the state equations corresponding to the switch-off state by the coefficient 1-D. It should be noted that the following assumption has been made:

$$x=[i_{L1}=x_1, i_{L2}=x_2, i_{Lf}=x_3,$$
$$v_{C1}=x_4, v_{C2}=x_5, v_{Cf}=x_6] \quad (5)$$

We express the system state equations in affine form.

$$\dot{x}=f(x)+g(x)D \quad (6)$$

$$f(x)=\begin{pmatrix} \frac{V_{in}-x_4}{L_1} \\ \frac{-x_5}{L_2} \\ \frac{x_4+x_5-x_6}{L_f} \\ \frac{x_1-x_3}{C_1} \\ \frac{x_2-x_3}{C_2} \\ \frac{R_L x_3-x_6}{C_f} \end{pmatrix},\ g(x)=\begin{pmatrix} \frac{x_4+x_5}{L_1} \\ \frac{x_4+x_5}{L_2} \\ \frac{-x_4-x_5}{L_f} \\ \frac{x_3-x_1-x_2}{C_1} \\ \frac{x_3-x_1-x_2}{C_1} \\ 0 \end{pmatrix} \quad (7)$$

VI. Dynamic analysis and controller Design

To design a linear controller for the QZSC, it is necessary to perform linearization around a specific operating point. To achieve linearization in equation (7), we replace the state variables and the duty cycle with the relations (8).

$$x_i=X_i+\tilde{x}_i\ (i=1\ to\ 6)$$
$$D=d+\tilde{d} \quad (8)$$

In equation (8), $\boldsymbol{X_i}$ represents the system's operating point, while $\boldsymbol{\tilde{x}_i}$ represents the disturbances around the operating point. Using the volt-second balance law for inductors, we can express the value of the state variables in steady state as equation (9).

$$\begin{cases} X_6=V_{ref}, D=\frac{V_{ref}-V_{in}}{2V_{ref}-V_{in}} \\ X_5=\frac{DV_{in}}{1-2D}, X_4=\frac{(1-D)V_{in}}{1-2D} \\ X_1=X_2=\frac{(1-D)V_{ref}}{(1-2D)R_{LOAD}}, X_3=\frac{V_{ref}}{R_{LOAD}} \end{cases} \quad (9)$$

By separating the different components and neglecting the product of small signal components (small signal approximation), we can obtain the linearized state-space model of the converter. It is important to note that when simplifying the derivative related to the system's operating point, it simplifies to zero. By utilizing this property, one can calculate the operating point of the system. By separating the matrix related to the states from the matrix related to the inputs, we can also derive the matrix of this converter. It should be noted that the product of two small signal values has been disregarded. The matrix of this converter can be expressed by equation (10).

$$\dot{\tilde{x}}=A\tilde{x}+B\tilde{d}$$

$$A=\begin{bmatrix} 0 & 0 & 0 & \frac{d-1}{L_1} & \frac{d}{L_1} & 0 \\ 0 & 0 & 0 & \frac{d}{L_2} & \frac{d-1}{L_2} & 0 \\ 0 & 0 & 0 & \frac{1-d}{L_f} & \frac{1-d}{L_f} & \frac{-1}{L_f} \\ \frac{1-d}{C_1} & \frac{d}{C_1} & \frac{d-1}{C_1} & 0 & 0 & 0 \\ \frac{-d}{C_2} & \frac{1-d}{C_2} & \frac{d-1}{C_2} & 0 & 0 & 0 \\ 0 & 0 & \frac{1}{C_f} & 0 & 0 & \frac{-1}{R_L C_f} \end{bmatrix}$$

$$B = \begin{bmatrix} \frac{x_4+x_5}{L_1} \\ \frac{x_4+x_5}{L_2} \\ \frac{-x_4-x_5}{L_f} \\ \frac{x_3-x_2-x_1}{C_1} \\ \frac{x_3-x_2-x_1}{C_2} \\ 0 \end{bmatrix} \quad (10)$$

In the representation of state space equations, C corresponds to the output vector of the system. In two situations, the transfer function of the system will be computed. When considering the inductor current and the output capacitor voltage, vector C in the standard state equations is represented as equation (11).

$$C_1 = [1\ 0\ 0\ 0\ 0\ 0]$$
$$C_6 = [0\ 0\ 0\ 0\ 0\ 1] \quad (11)$$

VII. Transfer functions of QZSC

The voltage transfer functions of the output filter capacitor and the inductor current with respect to the QZSC during the short circuit cycle will be calculated in the following calculations. These functions are denoted as H1 and H6, respectively. The following equation is utilized to calculate the aforementioned transfer functions. By applying the Laplace transform to equation (10) and utilizing the defined matrices C, we obtain:

$$H(s) = C(SI - A)^{-1}B + E \quad (12)$$

S is the Laplace variable. In equation (12), the variable I represents the 6x6 identity matrix, and E is the feedforward matrix of the system and its value is assumed to be zero.

The transfer functions of H1 and H6 are calculated based on the values given in Table 1. These transfer functions are represented by equation (13).

$$\begin{cases} H_1(s) = \frac{n_1(s)}{d_1(s)} \\ H_6(s) = \frac{n_6(6)}{d_1(s)} \\ n_1(s) = 1.5e6s^5 + 9.438e7s^4 + 3.416e13s^3 + 1.67e15s^2 \\ \quad +1.88e20s + 5.57e21 \\ n_6(s) = -4.412e9s^4 + 1.673e12s^3 - 5.49e16s^2 - \\ \quad 2.231e19s + 5.22e22 \\ d_1(s) = s^6 + 39.22s^5 + 2.307e7s^4 + 6.739e8s^3 + \\ \quad 1.301e14s^2 + 2.014e15s + 4.68e18 \end{cases} \quad (13)$$

TABLE.1. NOMINAL PARAMETERS OF QZSC

Parameters	Symbol	Value
Input voltage	V_{in}	50V
Network impedance inductors	L_1, L_2	0.5mH
Output filter inductor	L_f	1mH
Network impedance capacitors	C_1, C_2	150µF
Output filter capacitor	C_f	170µF
Output resistor	R_L	150Ω
Reference voltage	V_{ref}	500V
Switching frequency	f_s	50kHz

Upon calculating the zeros and poles of the H6 transfer function, it becomes evident that this function possesses zeros situated to the right of the imaginary axis. The positions of both the zeros and poles for the H1 and H6 transfer functions are depicted in Figure 4. Hence, it is not feasible to directly regulate the capacitor voltage as an output. The H1 transfer function is a minimum-phase transfer function, allowing for indirect control of the output voltage by manipulating the inductor current. Next, we will describe the process of creating a control loop to indirectly regulate the converter's output voltage.

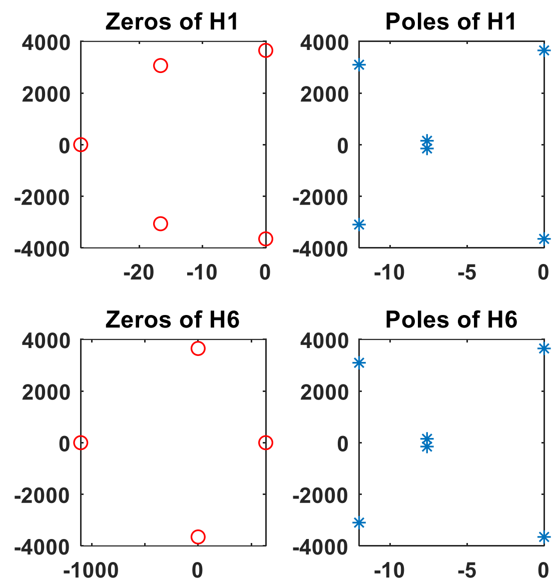

Fig. 4. Location of poles and zeros of QZSC transfer function

VIII. Indirectly controlling the output voltage of QZSC

Because the output capacitor voltage exhibits a non-minimum phase behavior and direct control is not possible, the voltage of the capacitor is indirectly regulated by manipulating the inductor current. Furthermore, considering the minimum-phase characteristic of the transfer function the inductor current to the duty cycle, the inductor current can be directly regulated by adjusting the duty cycle. The block diagram of the closed-loop system with the inclusion of the PI controller is depicted in Figure 5. The presented block diagram includes a pair of PI controllers.

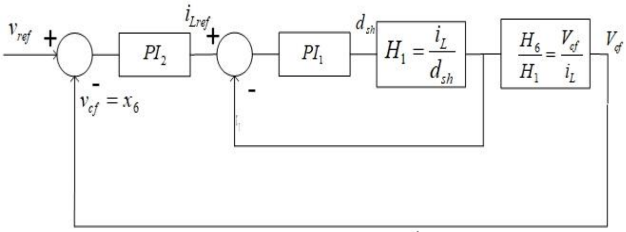

Fig. 5. Block diagram of the indirect control of the output voltage of the QZSC

The PI_1 controller receives the signal that is the difference between the impedance network's inductor current and its reference value. The output of the PI_1 controller represents the value of the duty cycle. The PI_2 controller selects the reference current value of the inductor according to the error between the reference voltage and the output voltage. The selection of these coefficients in this section has been done through a process of trial and error. The specific values of these coefficients are listed in Table 2. Smart algorithms can be employed to select coefficients that enable the control system to achieve desired values for evaluated parameters such as settling time, overshoot, undershoot, and steady-state error. Figure 6 illustrates the response of the block diagram when a reference voltage of 500V is chosen. The output reaches 500V after one undershoot and several overshoots. The controller design using the linearization method is relatively simple, but it does not ensure stability in a wide range. By changing the operating point, the linearized model is not valid and the output does not converge to the reference value. Hence, employing non-linear control methods is appropriate for the aforementioned system. Mr. Yutkin introduced the sliding mode control method for systems with variable structure. This method is widely used in power electronic systems because of their variable structure. The first step of the sliding mode control method is to define the sliding surface. The sliding mode control brings the system states to the sliding surface. When the system reaches the sliding surface, the sliding mode control maintains the system state close to and along the sliding surface. Usually, the sliding surface is defined as the output error of the system. After placing the answer on the surface, the system switches to the sliding mode. With proper switching, the response slides on the surface until it stabilizes.

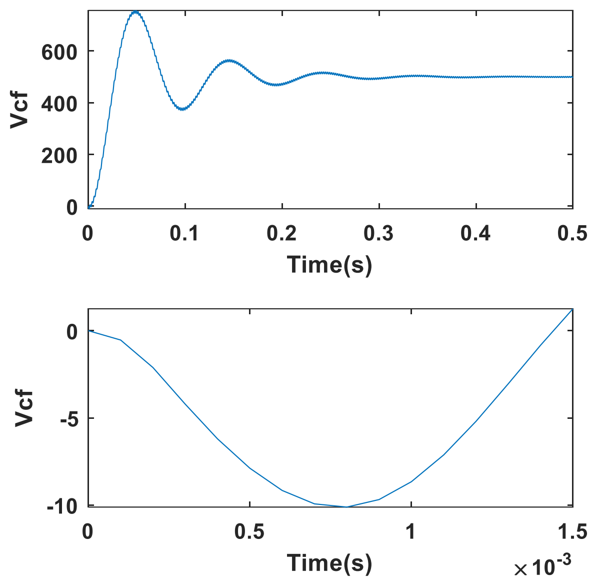

Fig.6. Step response of QZSC

TABLE. 2. SELECTED VALUES OF CONTROLLER COEFFICIENTS

controller coefficients	PI_1	PI_2
P	0.01	100
I	0.01	20

IX. Design of sliding mode controller in nominal condition

The sliding surface is defined by the current of the inductor in the impedance network. Equation (14) defines the sliding surface.

$$S = x_1^* - x_1 \quad (14)$$

The following definition is used to enter the output voltage in Equation (14).

$$x_1^* = K_I \int (x_6^* - x_6)dt \quad (15)$$

The output error is reduced to zero by including the integral factor. By substituting equation 15 into equation 14, we obtain the following result:

$$S = x_1^* - x_1 = K_I \int (x_6^* - x_6)dt - x_1 \quad (16)$$

Assuming that the sliding surface's derivative is zero, we can derive the equivalent controller.

$$\dot{S} = 0 \rightarrow \dot{x}_1^* - \dot{x}_1 = 0 \quad (17)$$

Using the state equations in equation (17), we can express the converter's short circuit cycle as equation (18).

$$D = \frac{K_I L_1 (x_6^* - x_6) + (x_4 - V_{in})}{x_4 + x_5} \quad (18)$$

Figure 7 presents the block diagram associated with the proposed control method.

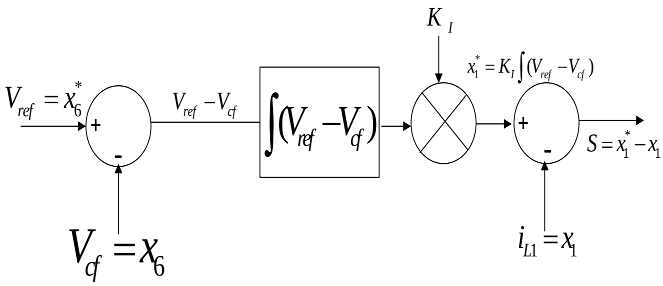

Fig.7. Block diagram of the proposed control method

By choosing the reference voltage and computing the duty cycle, the other state variables will be in the steady-state as equation (19).

$$\begin{cases} X_6 = V_{ref}, D = \frac{V_{ref}-V_{in}}{2V_{ref}-V_{in}} \\ X_5 = \frac{DV_{in}}{1-2D}, X_4 = \frac{(1-D)V_{in}}{1-2D} \\ X_1 = X_2 = \frac{(1-D)V_{ref}}{(1-2D)R_{LOAD}} \\ X_3 = \frac{V_{ref}}{R_{LOAD}} \end{cases} \quad (19)$$

X. Systematic selection of the integral coefficient on the sliding surface

By substituting equation (18) for the duty cycle into equations (6) and (7), we obtain the state equations in the form of equation (20):

$$\begin{cases} \dot{x}_1 = K_I(x_6^* - x_6),\ \dot{x}_2 = K_I(x_6^* - x_6) + \frac{x_4 - V_{in} - x_5}{L_2} \\ \dot{x}_3 = \frac{-K_I L_1 (x_6^* - x_6) + V_{in} + x_5 - x_6}{L_f} \\ \dot{x}_4 = \frac{K_I L_1 (x_6^* - x_6) + (x_4 - V_{in})}{x_4 + x_5} \left(\frac{x_3 - x_1 - x_2}{C_1}\right) + \\ \left(\frac{x_1 - x_3}{C_1}\right) \\ \dot{x}_5 = \frac{K_I L_1 (x_6^* - x_6) + (x_4 - V_{in})}{x_4 + x_5} \left(\frac{x_3 - x_1 - x_2}{C_2}\right) + \\ \left(\frac{x_2 - x_3}{C_2}\right),\ \dot{x}_6 = x_3 - \frac{x_6}{R_L} \end{cases} \quad (20)$$

Assuming that the changes around the operating point are small, we can linearize equation (20) around a specific operating point. We use the Jacobian method to linearize the system. The system under investigation has a 6x6 Jacobian matrix, and we can calculate its terms using equation (21).

$$\begin{cases} a_{ij} = \frac{\delta f_i}{\delta x_j}\ (i,j = 1,2,3,4,5,6) \\ \dot{x}_1 = f_1(x_1, x_2, x_3, x_4, x_5, x_6) \\ \dot{x}_2 = f_2(x_1, x_2, x_3, x_4, x_5, x_6) \\ \dot{x}_3 = f_3(x_1, x_2, x_3, x_4, x_5, x_6) \\ \dot{x}_4 = f_4(x_1, x_2, x_3, x_4, x_5, x_6) \\ \dot{x}_5 = f_5(x_1, x_2, x_3, x_4, x_5, x_6) \\ \dot{x}_6 = f_6(x_1, x_2, x_3, x_4, x_5, x_6) \end{cases} \quad (21)$$

The components of the Jacobian matrix are calculated according to equation (22). By substituting the system parameters and the desired operating point into equation (22), we obtain the Jacobian matrix as shown in equation (23). We note that the rest of the elements in the Jacobian matrix are zero. Using the Jacobian matrix that we computed, which depends on the integral gain, we can verify the system stability near the chosen operating point. We derive the system's characteristic equation from equation $|SI - A| = 0$. According to the Routh-Hurwitz stability criterion, the systems with $0 < K_I < 200$ are stable. The system's characteristic equation is given by equation (24). Within the given range, the system has all its poles on the left of the imaginary axis. S represents the Laplace variable in this context.

$$\begin{cases} a_{16} = a_{26} = -K_I, a_{25} = \frac{-1}{L_2}, a_{24} = \frac{1}{L_2} \\ a_{35} = \frac{1}{L_f}, a_{36} = \frac{K_I L_1 - 1}{L_f} \\ a_{41} = \frac{1}{C_1} - \frac{x_4 - V_{in} + K_I L_1 (x_6^* - x_6)}{C_1 (x_4 + x_5)} \\ a_{42} = \frac{-(x_4 - V_{in} + K_I L_1 (x_6^* - x_6))}{C_1 (x_4 + x_5)} \\ a_{43} = \frac{x_4 - V_{in} + K_I L_1 (x_6^* - x_6)}{C_1 (x_4 + x_5)} - \frac{1}{C_1} \\ a_{44} = \frac{(x_4 - V_{in} + K_I L_1 (x_6^* - x_6))(x_1 + x_2 - x_3)}{C_1 (x_4 + x_5)^2} - \\ \frac{x_1 + x_2 - x_3}{C_1 (x_4 + x_5)} \\ a_{45} = \frac{(x_4 - V_{in} + K_I L_1 (x_6^* - x_6))(x_1 + x_2 - x_3)}{C_1 (x_4 + x_5)^2} \\ a_{46} = \frac{K_I L_1 (x_1 + x_2 - x_3)}{C_1 (x_4 + x_5)} \\ a_{51} = -\frac{x_4 - V_{in} + K_I L_1 (x_6^* - x_6)}{C_2 (x_4 + x_5)} \\ a_{52} = \frac{1}{C_2} - \frac{x_4 - V_{in} + K_I L_1 (x_6^* - x_6)}{C_2 (x_4 + x_5)} \\ a_{53} = \frac{x_4 - V_{in} + K_I L_1 (x_6^* - x_6)}{C_2 (x_4 + x_5)} - \frac{1}{C_2} \\ a_{54} = \frac{(x_4 - V_{in} + K_I L_1 (x_6^* - x_6))(x_1 + x_2 - x_3)}{C_2 (x_4 + x_5)^2} \\ - \frac{x_1 + x_2 - x_3}{C_2 (x_4 + x_5)} \\ a_{55} = \frac{(x_4 - V_{in} + K_I L_1 (x_6^* - x_6))(x_1 + x_2 - x_3)}{C_2 (x_4 + x_5)^2} \\ a_{56} = \frac{K_I L_1 (x_1 + x_2 - x_3)}{C_2 (x_4 + x_5)} \\ a_{63} = 1,\ a_{66} = \frac{-1}{R_L} \end{cases} \quad (22)$$

$$A = \begin{pmatrix} 0 & 0 & 0 & 0 & 0 & -K_I \\ 0 & 0 & 0 & 2000 & -2000 & -K_I \\ 0 & 0 & 0 & 0 & 1000 & \frac{K_I}{2} - 1000 \\ 3.5 \times 10^3 & -3.2 \times 10^3 & -3.5 \times 10^3 & -233 & 211 & 0.22K_I \\ -3.2 \times 10^3 & 3.5 \times 10^3 & -3.5 \times 10^3 & -233 & 211 & 0.22K_I \\ 0 & 0 & 1 & 0 & 0 & -6.7 \times 10^3 \end{pmatrix} \quad (23)$$

$$S^6 + 23.4S^5 + (1.684 \times 10^7 - 0.5K_I)S^4 + (3.12 \times 10^8 - 233.9K_I)S^3 + (4.68 \times 10^{13} - 6.316 \times 10^6 K_I)S^2$$

$(6.238 \times 10^{11} - 3.119 \times 10^{9} K_I)S + 4.678 \times 10^{12} K_I = 0$ (24)

XI. Correction of Sliding Model Controller and Proof of Stability

The relation derived for the sliding mode controller in equation (18) is based on the nominal parameters of the model. To cope with model uncertainties, $K\ sgn(S)$ can be incorporated into the equivalent controller. To ensure that the sliding surface is absorbing, we define a Lyapunov function and verify the Lyapunov stability condition. We use equation (25) to define the Lyapunov function:

$$V(S) = \frac{1}{2} S^2 \quad (25)$$

The defined Lyapunov function has the initial condition of being positive definite. In order for the sliding surface to be absorbing, the derivative of the Lyapunov function must be negative definite.

$$\dot{V}(S) = S\dot{S} \leq -\eta |S| \quad (26)$$

We chooseη as a positive parameter for controlling the system.

$$\dot{S} = K_I(x_6^* - x_6) - D\frac{x_4 + x_5}{L_1} - \frac{V_{in} - x_4}{L_1} \quad (27)$$

We substitute the duty cycle with the following expression in equation (27):

$$D = \frac{K_I L_1 (x_6^* - x_6) + (x_4 - V_{in})}{x_4 + x_5} + Ksgn(S) \quad (28)$$

$$S(-Ksgn(S))\frac{x_4 + x_5}{L_1} \leq -\eta |S| \quad (29)$$

Considering that the value of $sgn(S) = |S|/S$ is the equation (29) is simplified as follows:

$$K \geq \frac{\eta L_1}{x_4 + x_5}, \eta > 0 \quad (30)$$

To summarize, the stability of the designed controller is ensured in a broad range of operating point and model uncertainties by selecting the control gain from equation (30). The designed controller has robustness to changes in load, input voltage and reference voltage. For instance, by choosing $\eta = 10$ and selecting the nominal operating points of the system using equation (19), we obtain a value of $K \geq 6 \times 10^{-6}$. However, in the simulations, we have opted for a value of $K = 10^{-5}$. According to equation (24), the coefficient $K_I = 100$ is considered.

TABLES.3. SETTLING TIME AND OVERSHOOT IN DIFFERENT MODES

Situation	Settling-time (s)		%O. V	
	increase	decrease	increase	decrease
Test 1	0.01	0.03	8	16
Test 2	0.006	0.02	3.98	1.52
Test 3	0.009	0.01	1.6	0.8

Figure 11 shows the block diagram where the control signal is applied to the converter. Within this diagram, the duty cycle derived from equation (28) regulates the converter's switch. This particular converter employs a unipolar switching technique.

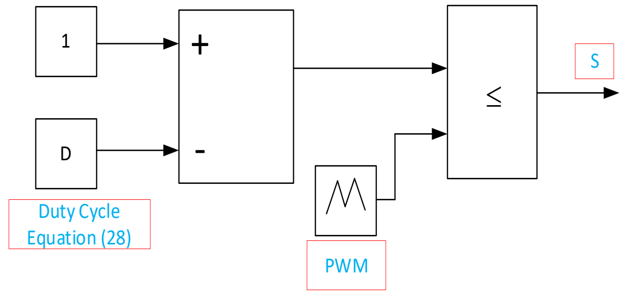

Fig.8. Shoot-through unipolar PWM technique

XII. Simulation results

This section presents simulations in MATLAB/Simulink software version 2018 that were performed to assess the performance of the suggested control technique. The system parameters of the QZSC are given in Table 1. The sampling time step for all the simulations is $1\mu s$. The following section examines how the designed controller responds to the variations of input voltage, load, and reference voltage. In Table 3, the control parameters, including settling time and overshoot, are calculated when changing the reference voltage, input voltage, and load.

Test1: This test considers the nominal values given in Table 1 and studies the step change in the output reference voltage. The output reference voltage increases from $V_{ref} = 500V$ to $V_{ref} = 550V$att $= 0.5s$and then decreases to $V_{ref} = 450V$at $t = 1s$. Figure 9 shows that the output voltage, V_o, can follow its reference value,V_{ref}. In this case output voltage error, defined by (31), tends zero in a finite time as shown in Figure 9.

$$V_{error} = V_{Cf} - V_{ref} \quad (31)$$

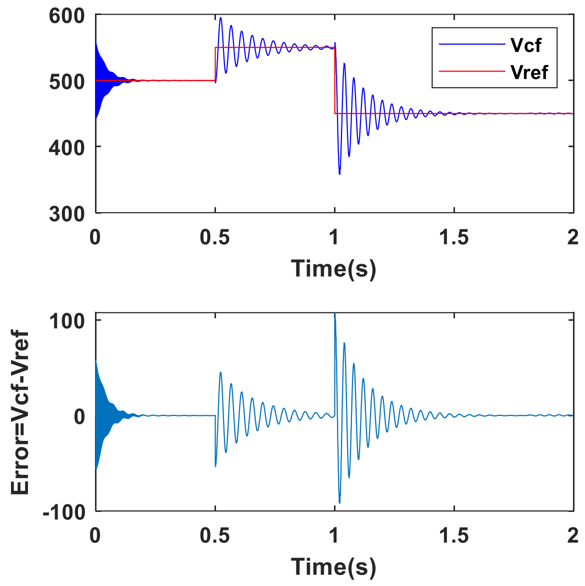

Fig.9. output reference voltage variation in test 1

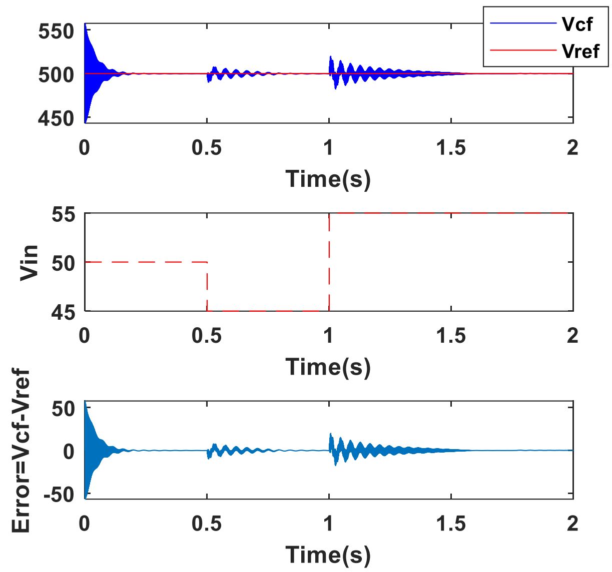

Fig.10. output reference voltage variation in test 2

Test2: To demonstrate the proposed controller's performance under input voltage disturbance, a step change in input voltage is applied. In this simulation, the input voltage is decreased to 45V in steps after 0.5s. As Figure 8 shows, the output voltage follows the reference voltage after a brief oscillation, and the steady state error is zero in this case. To enhance the impact of the input voltage on the output, this value is raised to 55V. Figure 10 shows that the output voltage reaches the reference value after a brief fluctuation. Figure 10 displays the variations in steady state error and input voltage. The results demonstrate the stability of the proposed control system under varying input voltage. Table 3 displays the results obtained by varying the input voltage. Specifically, during the increase and decrease phases, the overshoot values are 3.98 and 1.52, respectively. These findings demonstrate that the presented control system exhibits robustness to fluctuations in the input voltage.

Test3: This simulation verifies the robustness of the proposed controller under varying load conditions. The output resistance is decreased from 150Ω to 135Ω after 0.5s. Figure 11 shows the result of this change. Figure 11 shows that the output voltage reaches the initial reference voltage within 0.5s of the simulation. To examine the effect of higher output resistance on the output voltage, this value is raised to 165Ω. This change occurs 1s into the simulation. Figure 11 also presents the result of this change. Figure 11 illustrates that the output voltage matches the reference voltage quickly after the resistance increases. Hence, the proposed controller can track the reference voltage despite variations in the output resistance. Based on Table 3, the settling time and overshoot values during both the increase and decrease phases of the output load fall within an acceptable range. As a result, the provided controller exhibits robustness in load variations.

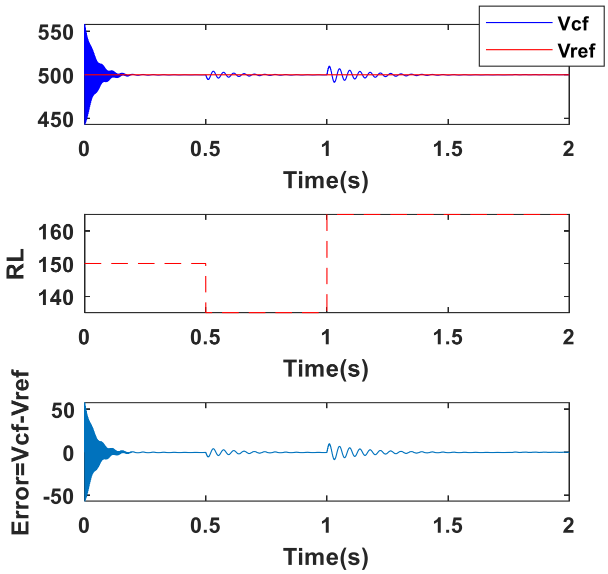

Fig .11. output reference voltage variation in test 3

Test4: This simulation explores the effect of changing the reference voltage, input voltage, and output resistance at the same time. After 0.5s from the beginning of the simulation, the reference voltage was lowered to 450V, the input voltage to 45V, and the output resistance to 135Ω. Figure12 demonstrate the results of these changes. The output could track the reference voltage and reached 450V quickly. One second after the simulation begins, the reference voltage rises to 550V, the input voltage goes up to 55V, and the output resistance grows to 165Ω. The output followed the reference voltage as the parameters increased at the same time, and it attained 550V in a brief period.

XIII. Conclusion

In this study, we investigated the equivalent sliding mode control of a DC-DC QZSC with an output filter. The principles of step-by-step design for the sliding mode controller and the selection criteria for the control coefficients in the sliding mode method are presented in detail. In the studied system, the output capacitor voltage to the duty cycle of the converter is nonminimum phase. This means we cannot control the output voltage directly by changing the duty cycle. To address this issue, we used a sliding surface defined as the proportion of the difference between the QZSC's inductor current and its reference value. Based on simulations conducted in both transient and permanent modes, the designed sliding mode controller exhibits robustness in response to changes in load and input voltage. The percentage of response overshoot in reference voltage change exceeds that of both load and input voltage changes. Furthermore, in accordance with the system's reference voltage definition, the output error remains zero throughout all tests. The proposed controller ensures local asymptotic stability. The potential for a universal asymptotic controller for the desired system can be explored in further research.

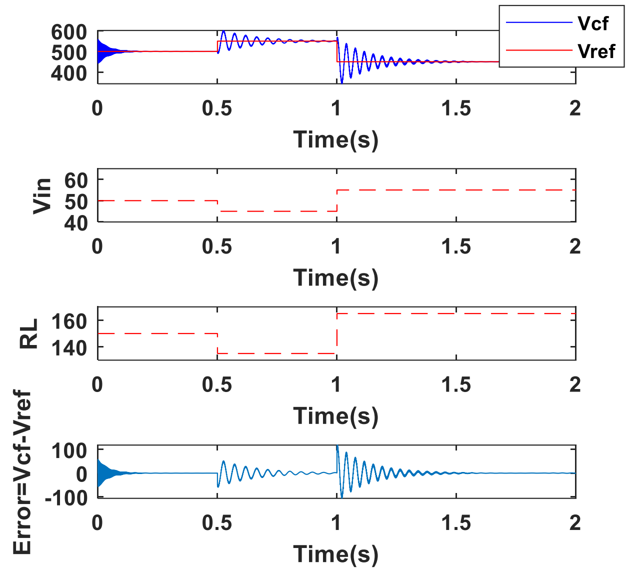

Fig. 12. output reference voltage variation in test 4

References:

[1] N. Javaid *et al.*, "An intelligent load management system with renewable energy integration for smart homes," *IEEE access*, vol. 5, pp. 13587-13600, 2017.

[2] W. Tushar, J. A. Zhang, C. Yuen, D. B. Smith, and N. U. Hassan, "Management of renewable energy for a shared facility controller in smart grid," *IEEE Access*, vol. 4, pp. 4269-4281, 2016.

[3] X. Zhu and B. Zhang, "High step-up quasi-Z-source DC-DC converters with single switched capacitor branch," *Journal of Modern Power Systems and Clean Energy*, vol. 5, no. 4, pp. 537-547, 2017.

[4] S. Padmanaban, P. K. Maroti, J. B. Holm-Nielsen, F. Blaabjerg, Z. Leonowicz, and V. Yaramasu, "Quazi Z-source single stage high step-up DC-DC converter for grid-connected PV application," in *2019 IEEE International Conference on Environment and Electrical Engineering and 2019 IEEE Industrial and Commercial Power Systems Europe (EEEIC/I&CPS Europe)*, 2019, pp. 1-6: IEEE.

[5] P. Padmavathi and S. Natarajan, "Single switch quasi Z-source based high voltage gain DC-DC converter," *International Transactions on Electrical Energy Systems*, vol. 30, no. 7, p. e12399, 2020.

[6] F. Z. Peng, "Z-source inverter," *IEEE Transactions on industry applications*, vol. 39, no. 2, pp. 504-510, 2003.

[7] J. Anderson and F. Z. Peng, "Four quasi-Z-source inverters," in *2008 IEEE Power Electronics Specialists Conference*, 2008, pp. 2743-2749: IEEE.

[8] G. R. Shahabadi, M. R. Naseh, and S. Es' haghi, "Analysis and design of switched capacitor-based Quasi-Z-Source DC-DC converter with improved operation factors," *International Journal of Electronics*, pp. 1-20, 2023.

[9] S. Laali and E. Babaei, "Developed Quasi Z-Source Inverters Based on Diode-Cells: Analysis and

Implementation," *International Journal of Industrial Electronics Control and Optimization*, vol. 5, no. 1, pp. 51-62, 2022.

[10] A. Karbalaei, M. Mardaneh, and M. Shasadeghi, "A new topology of the switched-inductor/capacitor quasi Z-source inverter with ability of uplifted-boost," *International Journal of Industrial Electronics Control and Optimization*, vol. 3, no. 1, pp. 35-46, 2020.

[11] M. K. Kazimierczuk, "Small-signal modeling of open-loop PWM Z-source converter by circuit-averaging technique," *IEEE Transactions on Power Electronics*, vol. 28, no. 3, pp. 1286-1296, 2012.

[12] S. Samanta, S. Barman, J. P. Mishra, P. Roy, and B. K. Roy, "Design of an interconnection and damping assignment-passivity based control technique for energy management and damping improvement of a DC microgrid," *IET Generation, Transmission & Distribution*, vol. 14, no. 11, pp. 2082-2091, 2020.

[13] M. Salimi and S. Siami, "Cascade nonlinear control of DC-DC buck/boost converter using exact feedback linearization," in *2015 4th International Conference on Electric Power and Energy Conversion Systems (EPECS)*, 2015, pp. 1-5: IEEE.

[14] A. A. Chlaihawi, A. M. Al-Modaffer, and Z. Alhadrawi, "Performance analysis of different methods for optimal sliding mode control of DC/DC buck converter," *Bulletin of Electrical Engineering and Informatics*, vol. 13, no. 1, pp. 117-124, 2024.

[15] N. Mukherjee and D. Strickland, "Control of cascaded DC–DC converter-based hybrid battery energy storage systems—Part II: Lyapunov approach," *IEEE Transactions on Industrial Electronics*, vol. 63, no. 5, pp. 3050-3059, 2015.

[16] F. Bagheri, H. Komurcugil, O. Kukrer, N. Guler, and S. Bayhan, "Multi-input multi-output-based sliding-mode controller for single-phase quasi-Z-source inverters," *IEEE Transactions on Industrial Electronics*, vol. 67, no. 8, pp. 6439-6449, 2019.

[17] M. Bensaada and A. B. Stambouli, "A practical design sliding mode controller for DC–DC converter based on control parameters optimization using assigned poles associate to genetic algorithm," *International Journal of Electrical Power & Energy Systems*, vol. 53, pp. 761-773, 2013.

[18] S. H. Chincholkar and C.-Y. Chan, "Design of fixed-frequency pulsewidth-modulation-based sliding-mode controllers for the quadratic boost converter," *IEEE Transactions on Circuits and Systems II: Express Briefs*, vol. 64, no. 1, pp. 51-55, 2016.

[19] S. Ahmadzadeh, G. A. Markadeh, and N. Abiadi, "Adaptive sliding mode control of step-up/step-down Z-source DC-DC converter," in *2019 27th Iranian Conference on Electrical Engineering (ICEE)*, 2019, pp. 841-845: IEEE.

[20] H. Zaman, X. Zheng, S. Khan, H. Ali, and X. Wu, "Hysteresis modulation-based sliding mode current control of Z-source DC-DC converter," in *2016 IEEE 8th International Power Electronics and Motion Control Conference (IPEMC-ECCE Asia)*, 2016, pp. 321-324: IEEE.

[21] S. Ahmadzadeh, G. A. Markadeh, and N. Abjadi, "Back-stepping sliding mode control of a Z-source DC-DC converter," in *2018 9th Annual Power Electronics, Drives Systems and Technologies Conference (PEDSTC)*, 2018, pp. 414-418: IEEE.

[22] Y. Zhang, Q. Liu, J. Li, and M. Sumner, "A Common Ground Switched-Quasi-$ Z $-Source Bidirectional DC–DC Converter With Wide-Voltage-Gain Range for EVs With Hybrid Energy Sources," *IEEE Transactions on Industrial Electronics*, vol. 65, no. 6, pp. 5188-5200, 2017.

[23] S. Ahmadzadeh, G. A. Markadeh, and N. Abjadi, "Sliding mode control of the four quadrant quasi-Z-Source DC-DC Converter," in *2017 8th Power Electronics, Drive Systems & Technologies Conference (PEDSTC)*, 2017, pp. 496-501: IEEE.

[24] A. H. Rajaei, S. Kaboli, and A. Emadi, "Sliding-mode control of Z-source inverter," in *2008 34th Annual Conference of IEEE Industrial Electronics*, 2008, pp. 947-952: IEEE.

[25] J. R. Gazoli, M. G. Villalva, and E. Ruppert, "Micro-inverter for integrated grid-tie photovoltaic module using resonant controller," *International Transactions on Electrical Energy Systems*, vol. 24, no. 5, pp. 713-722, 2014.

[26] Y. P. Siwakoti, F. Z. Peng, F. Blaabjerg, P. C. Loh, G. E. Town, and S. Yang, "Impedance-source networks for electric power conversion part II: Review of control and modulation techniques," *IEEE Transactions on Power Electronics*, vol. 30, no. 4, pp. 1887-1906, 2014.

[27] Y. Tang and S. Xie, "System design of series Z-source inverter with feedforward and space vector pulse-width modulation control strategy," *IET Power Electronics*, vol. 7, no. 3, pp. 736-744, 2014.

[28] S. Rostami, V. Abbasi, and F. Blaabjerg, "Implementation of a common grounded Z-source DC–DC converter with improved operation factors," *IET Power Electronics*, vol. 12, no. 9, pp. 2245-2255, 2019.

[29] J. A. Ruz-Hernandez, R. Garcia-Hernandez, M. A. Ruz Canul, J. F. Guerra, J.-L. Rullan-Lara, and J. R. Vior-Franco, "Neural Sliding Mode Control of a Buck-Boost Converter Applied to a Regenerative Braking System for Electric Vehicles," *World Electric Vehicle Journal*, vol. 15, no. 2, p. 48, 2024.

[30] A. Zakipour, S. Shokri-Kojori, and M. Tavakoli Bina, "Sliding mode control of the nonminimum phase grid-connected Z-source inverter," *International Transactions on Electrical Energy Systems*, vol. 27, no. 11, p. e2398, 2017.

[31] M. Salimi, "A novel approach for sliding mode controller design and parameters selection in flyback switching power supplies," Journal of Iranian Association of Electrical and Electronics Engineers, 1 vol. 16, no. 3, pp. 1-12, 2019.[In Pesian]

[32] H. B. Nouzadan, M. Babaei, and A. Ibrahim, "A novel multilevel structure for impedance source inverters," Journal of Iranian Association of Electrical and Electronics Engineers, vol. 15, no. 1, pp. 75-87, 2018. [In Persian].

[33] S. Eslami, A. Siadat, and M. Javani, "Design and simulation of an interleaved parallel boost DC-DC converter with soft switching for application in renewable energy sources," Journal of Iranian Association of Electrical and Electronics Engineers, vol. 19, no. 2, pp. 149-158, 2022. [In Persian].

Gholamreza Shahabadi was born in Birjand in 1983. He obtained his MS degree from the Faculty of Engineering at Islamic Azad University, Gonabad branch, Iran, in 2008. Later, he pursued his PhD degree in Electrical Engineering at the Islamic Azad University, Birjand branch, Iran, in 2024. Since 2013, he has been working at the University of Applied Science and Technology, South Khorasan Branch, Iran, where his research field focuses on DC-DC converters.

Majid Reza Naseh was born in Mashhad, Iran, in 1970. He earned his M.S. degree from the Faculty of Engineering at Islamic Azad University, South Tehran branch, Iran, in 1995. Later, he pursued his Ph.D. degrees in Electrical Engineering at the Islamic Azad University, Science and Research branch, Tehran, Iran, completing them in 2008. In 1998, he joined the Islamic Azad University, Birjand branch, where he began his academic career as an Instructor in the Department of Electrical Engineering. Since 2008, he has held the position of Assistant Professor. His research interests encompass a wide range of topics, including power electronic converters, power system operation and control, and hybrid renewable energy systems.